Supplementary information

Efficient Capture of Sr^{2+} Ions by a Layered Crystalline Zirconium Phosphate Fluoride

Ziyuan Chen [a,b,c], Shuzhen Liu [b,c], Shuangjiang Li [b,c], Zhihua Chen [b,c], Lu Yang [b,c], Shengmao Zhang [a], Haiyan Sun [b,c,*], Meiling Feng [b,c,*] and Xiaoying Huang [b,c]

[a.] *College of Chemistry and Materials Science, Fujian Normal University, Fuzhou 350007, P. R. China*

[b.] *State Key Laboratory of Structural Chemistry, Fujian Institute of Research on the Structure of Matter, Chinese Academy of Sciences, Fuzhou 350002, P. R. China*

[c.] *Fujian College, University of Chinese Academy of Sciences, Fuzhou, 350002, P.R. China*

† shy@fjirsm.ac.cn (H. Y. Sun); fml@fjirsm.ac.cn (M. L. Feng)

1. Batch adsorption experiments.

(1) Isothermal Adsorption Experiments

Sr^{2+} solutions with gradient initial concentrations (C_0 = 28.84 - 1000.42 mg L^{-1}) were subjected to equilibrium studies. A fixed solid-to-liquid ratio (m/V = 1 g L^{-1}; m = 10 mg adsorbent, V = 10 mL solution) was maintained. After 12 h agitation (25 ± 1°C), suspensions were filtered through 0.22 μm membranes. The filtrates were acidified with 2% HNO_3 (*v*/*v*) prior to Sr^{2+} quantification via ICP-MS/OES.

(2) Adsorption Kinetic Experiments

A 50 mg of $[(CH_3)_2NH_2][Zr(PO_4)F_2]$ powder was introduced into 50 mL Sr^{2+} solution (C_0 = 34.04 mg L^{-1}). Aliquots (1 mL) were extracted at predetermined time intervals (t = 1 - 1440 min), immediately filtered, and analyzed by ICP-MS to determine residual Sr^{2+} concentrations (C_t). The pseudo-first-order model and pseudo-second-order model were fitted to kinetic data.

(3) pH Effect Experiments

The pH of Sr^{2+} solutions (C_o = 11.12 - 14.15 mg L^{-1}) was adjusted from 0.92 to 12.92 using 0.1 M HNO_3/NaOH. Adsorption proceeded for 12 h at m/V = 1 g L^{-1} (25 ± 1°C). Post-filtration acidification and ICP-MS analysis followed the isotherm protocol. The dissolution concentrations of Zr were measured by ICP-MS. Then, we employed the pH drift method for analyzing the pH dependence of adsorption. 10 mg of $[(CH_3)_2NH_2][Zr(PO_4)F_2]$ was immersed for 12 hours in 10 mL aqueous solutions with a pH range of 0.97-13.11, and then the solutions pH was recorded. The initial pH value was then compared to the triangular pH value.

(4) Competitive Adsorption Experiments

Selectivity was evaluated in multicomponent systems (containing Na^+, K^+, Cs^+, Ca^{2+}, and Mg^{2+} ions) and actual aqueous systems such as seawater (Dongshan Island, Zhangzhou, Fujian, China), tap water (Wulong River, Fuzhou, Fujian, China), river water (Wulong River, Fuzhou, Fujian, China), and lake water (Qishan Lake, Fuzhou, Fujian, China). Sr^{2+} concentration (C_0 = 3.15 - 6.59 mg L^{-1}) and m/V = 1 g L^{-1} were employed. Competitive distribution coefficients (K_d^{Sr}) and removal rate (R^{Sr}) were calculated after 12 h contact.

(5) Adsorption-Desorption Experiments

The $[(CH_3)_2NH_2][Zr(PO_4)F_2]$ adsorbent (50 mg) was equilibrated with 50 mL Sr^{2+} solution (nominal concentration: 1000 mg L^{-1}) for 12 h at 25 °C to yield Sr^{2+}-loaded $[(CH_3)_2NH_2][Zr(PO_4)F_2]$ (denoted $[(CH_3)_2NH_2][Zr(PO_4)F_2]$-Sr). Subsequently, 20 mg aliquots of $[(CH_3)_2NH_2][Zr(PO_4)F_2]$-Sr were immersed in 20 mL eluent solutions (0.5 mol L^{-1} KCl) under continuous agitation (200 rpm) for 12 h at ambient temperature. Post-treatment, the solid phases were recovered via vacuum filtration (0.22 μm membrane), air-dried at 25 °C, and subjected to powder X-ray diffraction. The filtrates were acidified with 2% HNO_3 (*v*/*v*) for Sr^{2+} desorption quantification by ICP-MS.

(6) Thermodynamic Experiments

The $[(CH_3)_2NH_2][Zr(PO_4)F_2]$ adsorbent (10 mg) was added to 10 mL Sr^{2+} solutions (initial concentration: 9.82 - 10.39 mg L^{-1}). The mixtures were magnetically stirred for 12 h at controlled temperatures (293, 313, 333 K). Post-adsorption solutions were diluted appropriately and analyzed by ICP-MS for residual Sr^{2+} concentration.

2. Equations.

The equations for the analysis of adsorption experiments are summarized as follows:

(1) The adsorption capacity q (mg g^{-1}) can be calculated according to Eq. S1.

$$q = \frac{(C_0 - C_e)V}{m} \quad \text{(Eq. S1)}$$

C_0 (mg L^{-1}) and C_e (mg L^{-1}) are the initial and equilibrium concentration of target ions, respectively. The m (g) and V (mL) are the mass of the adsorbent and the volume of the solution used in the adsorption experiment, respectively.

The theoretical adsorption capacity can be calculated according to Eq. S2.

$$q(theoretical) = \frac{One\ half\ of\ atomic\ weight\ of\ strontium}{Formula\ weight\ of\ adsorbent} \times 1000 \quad \text{(Eq. S2)}$$

(2) Eq. S3, S4 and S5 represent the classical isotherm models, namely the Langmuir, Langmuir-Freundlich and Freundlich models [1], which are used to evaluate the maximum adsorption capacity (q_m) of the adsorbent for a target ion.

$$q = q_m \frac{bC_e}{1 + bC_e} \quad \text{(Eq. S3)}$$

$$q = q_m \frac{(K_L C_e)^{\frac{1}{n}}}{1 + (K_L C_e)^{\frac{1}{n}}} \quad \text{(Eq. S4)}$$

$$q = K_F C_e^{\frac{1}{n}} \quad \text{(Eq. S5)}$$

The q_m is the maximum adsorption capacity (mg g^{-1}); b is the Langmuir constant related to the affinity of the ion for the adsorbent (L mg^{-1}), and n is the density constant at the adsorption site. K_F ($mg^{1-1/n} \cdot L^{1/n}/g$) is the fitting parameter related to the adsorption capacity.

(3) The removal rate R (%) can be calculated according to Eq. S6.

$$R = \frac{(C_0 - C_e)}{C_0} \times 100\% \quad \text{(Eq. S6)}$$

(4) Kinetics models are shown in Eq. S7 and S8 [2].

$$ln\frac{(q_e - q))}{q_e} = -k_1 t \quad \text{(Eq. S7)}$$

$$\frac{t}{q} = \frac{1}{k_2 q_e^2} + \frac{1}{q_e} t \quad \text{(Eq. S8)}$$

The k_1 and k_2 are pseudo-first-order and the pseudo-second-order rate constants of kinetics models, respectively. The pseudo-second-order rate expression has been widely applied to the adsorption of pollutants from aqueous solutions.

(5) The distribution coefficient K_d (mL g^{-1}) can be calculated according to Eq. S9.

$$K_d = \frac{V(C_0 - C_e)}{m \quad C_e} \qquad \text{(Eq. S9)}$$

(6) Leaching rate (R_L)

$$R_L = \frac{C_P}{C_T} \times 100\% \quad \text{(Eq. S10)}$$

Where R_L(%) is the leaching rate, C_P (mg L^{-1}) is the concentration of Zr ions in the solution after soaking the $[(CH_3)_2NH_2][Zr(PO_4)F_2]$, and C_T (mg L^{-1}) is the theoretical concentration of Zr ions when $[(CH_3)_2NH_2][Zr(PO_4)F_2]$ is completely dissolved in the solution.

(6) Separation factor (*SF*)

$$SF = \frac{K_d^A}{K_d^B} \quad \text{(Eq. S11)}$$

In this equation, K_d^A and K_d^B represent the distribution coefficients of *A* and *B* ions, respectively.

(7) The desorption rate can be considered as the percentage of the mass of Sr^{2+} ions desorbed off to the mass of Sr^{2+} ions adsorbed on, but considering the loss of solid mass, it can be calculated by the following equation:

$$E = \frac{C_e^{de} V_{de}}{m_2 (m_{Sr}^{ad}/m_{ad})} \times 100\% \quad \text{(Eq. S12)}$$

where C_e^{de} (mg L^{-1}) is the Sr^{2+} concentration in the solution after desorption, V_{de} (L) is the volume of solution used during desorption. M_{Sr}^{ad} (mg) is the mass of adsorbed Sr^{2+} ion during the adsorption process, and m_{ad} (mg) is the mass of the solid sample after adsorption of Sr^{2+}, m_2 (mg) is the mass of the solid sample used during desorption.

(8) The thermodynamic parameter Gibbs free energy change (Δ*G*) can be calculated using Eq. S13. The relationship among Δ*G*, entropy change (Δ*S*), and enthalpy change (Δ*H*) is described by Eq. S14. Combined with Equations Eq. S13 and Eq. S14, the van't Hoff equation (Eq. S15) is derived. Thermodynamic parameters were determined as follows [3, 4]:

$$\Delta G^0 = -RT\ln K_C \quad \text{(Eq. S13)}$$

$$\Delta G^0 = \Delta H^0 - T\Delta S^0 \quad \text{(Eq. S14)}$$

$$\ln K_C = -\frac{\Delta H^0}{RT} + \frac{\Delta S^0}{R} \quad \text{(Eq. S15)}$$

where K_C denotes the equilibrium constant, *R* is the ideal gas constant (8.314 J mol^{-1} K^{-1}), and *T* represents the absolute temperature in Kelvin (K).

3. Crystal structures section.

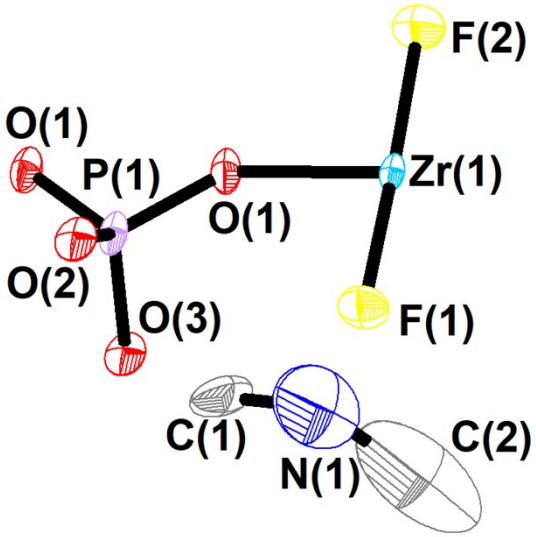

Figure S1. *ORTEP* plot (50% ellipsoid probability) showing the crystallographically asymmetric unit of $[(CH_3)_2NH_2][Zr(PO_4)F_2]$. Hydrogen atoms are omitted for clarity.

* The above data are all from the corresponding CIF files. Interlayer spacing quantification in $[(CH_3)_2NH_2][Zr(PO_4)F_2]$ was performed using *Diamond* crystallographic software through the following protocol (Figure 1e): (1) Selection of three non-coplanar Zr atoms defining the anionic basal plane; (2) construction of a least-squares orthogonal plane from these reference atoms; (3) measurement of perpendicular distance ($d\perp$) from each Zr site in adjacent layers to the reference plane).

Table S1. Crystallographic data and refinement details for $[(CH_3)_2NH_2][Zr(PO_4)F_2]$.

Compound	**$[(CH_3)_2NH_2][Zr(PO_4)F_2]$**
Empirical formula	$C_2H_8F_2NO_4PZr$
Formula weight	270.28
Temperature/K	100
Crystal system	monoclinic
Space group	$P2_1/m$
a/Å	6.5946(10)
b/Å	6.5775(11)
c/Å	9.962(3)
α/°	90
β/°	98.763(18)
γ/°	90
V/Å^3	427.07(16)
Z	2
ρ_{calc} g cm^{-3}	2.102
μ/mm^{-1}	1.480
F (000)	264.0
Crystal size/mm^3	0.20 × 0.10 × 0.05
Radiation	MoK_α (λ = 0.71073 Å)
2θ range for data collection/°	6.252 to 52.73
Index ranges	-8 <= h <= 7, -8 <= k <= 7, -10 <= l <= 12
Reflections collected	3341
Independent reflections	951 [R_{int} = 0.1117, R_{sigma} = 0.1033]
Data/restraints/parameters	951/20/75
Goodness-of-fit on F^2	1.097
Final R indexes [I>=2σ(I)]	R_1 = 0.0559, wR_2 = 0.1330
Final R indexes [all data]	R_1 = 0.0714, wR_2 = 0.1477
Largest diff. peak/hole/eÅ^{-3}	1.18/-1.14
CCDC	2466544

[a] $R_1 = \sum \| F_o| - |F_c \| / \sum |F_o|$, $wR_2 = [\sum w(F_o^2 - F_c^2)^2 / \sum w(F_o^2)^2]^{1/2}$.

Table S2. Selected bond distances (Å) and angles (°) for $[(CH_3)_2NH_2][Zr(PO_4)F_2]$.

Zr(1)-F(1)	1.972(6)	Zr(1)-O(3)#2	2.054(5)	P(1)-O(1)#4	1.528(4)
Zr(1)-F(2)	2.007(6)	Zr(1)-O(3)#3	2.079(5)	P(1)-O(2)	1.534(7)
Zr(1)-O(1)#1	2.054(4)	P(1)-O(3)	1.527(5)	N(1)-C(2)	1.471(19)
Zr(1)-O(1)	2.054(4)	P(1)-O(1)	1.528(4)	N(1)-C(1)	1.52(2)
F(1)-Zr(1)-F(2)	176.0(2)	O(1)#1-Zr(1)-O(1)	177.2(3)	O(3)-P(1)-O(2)	107.0(4)
F(1)-Zr(1)-O(1)#1	89.10(13)	O(1)#1-Zr(1)-O(3)#2	91.11(10)	O(1)-P(1)-O(2)	110.7(2)
F(1)-Zr(1)-O(1)#1	90.82(13)	O(1)-Zr(1)-O(3)#2	91.11(10)	O(1)#4-P(1)-O(2)	110.7(2)
F(1)-Zr(1)-O(1)	89.10(13)	O(1)#1-Zr(1)-O(2)#3	88.89(10)	P(1)-O(1)-Zr(1)	144.8(3)
F(2)-Zr(1)-O(1)	90.82(13)	O(1)-Zr(1)-O(2)#3	88.89(10)	P(1)-O(2)-Zr(1)#3	142.6(4)
F(1)-Zr(1)-O(3)#2	90.5(2)	O(3)#2-Zr(1)-O(2)#3	179.9(3)	P(1)-O(3)-Zr(1)#2	144.5(5)
F(2)-Zr(1)-O(3)#2	93.5(3)	O(3)-P(1)-O(1)	110.3(2)	C(2)-N(1)-C(1)	119(3)
F(1)-Zr(1)-O(2)#3	89.4(2)	O(3)-P(1)-O(1)#4	110.2(2)		
F(2)-Zr(1)-O(2)#3	86.6(3)	O(1)-P(1)-O(1)#4	108.0(4)		

* Symmetry Codes: #1 +*x*,1/2-*y*,+*z*; #2 1-*x*,1-*y*,1-*z*; #3 -*x*,1-*y*,1-*z*; #4 +*x*,3/2-*y*,+*z*.

Table S3. Hydrogen bonds between $[(CH_3)_2NH_2]^+$ cations and the anionic layers in $[(CH_3)_2NH_2][Zr(PO_4)F_2]$.

D-H···A	d(D-H) (Å)	d(H···A) (Å)	d(D···A) (Å)	<(DHA) (°)
N(1)-H(1B)···F(2)#1	0.91	2.65	3.37(4)	137.3
C(1)-H(1C)···O(2)#2	0.98	2.70	3.58(4)	150.4
C(2)-H(2A)···F(2)#3	0.98	2.05	2.99(2)	160.1
C(2)-H(2B)···F(1)	0.98	1.82	2.63(3)	138.4

* Symmetry Codes: #1 +*x*,+*y*,1+*z*; #2 +*x*,-1+*y*,+*z*; #3 -*x*,1-*y*,1-*z*.

4. Characterizations section

Table S4. Experimental results of the adsorption capacity study of $[(CH_3)_2NH_2][Zr(PO_4)F_2]$ (m/V = 1 g L^{-1}, at room temperature and 12 h contact time).

C_0^{Sr} (mg L^{-1})	C_e^{Sr} (mg L^{-1})	q_e^{Sr} (mg g^{-1})
28.84	0.95	27.89
50.78	1.27	49.51
100.36	10.05	90.31
149.62	22.20	127.42
227.99	85.71	142.28
442.53	289.85	152.68
708.62	553.52	155.10
1000.42	841.46	158.96

Table S5. Adsorption constants obtained by fitting isotherm data to $[(CH_3)_2NH_2][Zr(PO_4)F_2]$ using the Langmuir, Langmuir-Freundlich, and Freundlich models.

Adsorption isotherm model	Langmuir model	Langmuir-Freundlich model	Freundlich model
R^2	0.9699	0.9858	0.8467
q_m^{Sr} (mg g^{-1})	154.16 ± 5.00	161.48 ± 5.99	-
b (L mg^{-1})	0.21 ± 0.045	0.18 ± 0.038	-
n	-	1.34 ± 0.18	6.34 ± 1.36
k_F	-	-	60.11 ± 11.08

Table S6. Comparison of the adsorption capacities of $[(CH_3)_2NH_2][Zr(PO_4)F_2]$ and some other reported inorganic adsorbents for Sr^{2+}.

Materials	q_m^{Sr} (mg g^{-1})	Ref.
$[(CH_3)_2NH_2][Zr(PO_4)F_2]$	161.48	This work
$[(CH_3)_2NH_2]_2[ZrC_6H_4(CH_2PO_3)_2F_2]$ (SZ-7)	129.1	[5]
$[(CH_3)_2NH_2][ZrCH_2(PO_3)_2F]$ (SZ-4)	121	[6]
$[(CH_3)_2NH_2]_2[Zr(CH_2(HPO_3)(PO_3))_2$ (SZ-5)	118.6	[7]
γ-$Zr(PO_4)H_2PO_4{\cdot}2H_2O$ (γ-ZrP)	114.78	[8]
$K_{2x}Sn_{4-x}S_{8-x}$ (x = 0.65-1) (KTS-3)	102.00	[9]
$K_{2x}Mg_xSn_{3x}S_6$ (x = 0.5-1) (KMS-2)	86.89	[10]
$K_{2x}Mn_xSn_{3-x}S_6$ (x = 0.5-0.95) (KMS-3)	77.00	[11]
$[Me_2NH_2]_{4/3}[Me_3NH]_{2/3}Sn_3S_7{\cdot}1.25H_2O$ (FJSM-SnS)	65.19	[12]
$K_2Zr[CH_2(PO_3)_2]F_2$ (SZ-8)	55	[13]
$K_2Zr(PO_4)_2$	52.83	[14]
α-$Zr(HPO_4)_2{\cdot}H_2O$ (α-ZrP)	43.03	[15, 16]
ZrO_2-Sb_2O	22.21	[17]
AMP-PAN	16.00	[18]

Table S7. The Sr^{2+} adsorption kinetics results of $[(CH_3)_2NH_2][Zr(PO_4)F_2]$ (m/V = 1 g L^{-1}, at room temperature).

t (min)	C_t^{Sr} (mg L^{-1})	R^{Sr} (%)
0	34.04	0.00
1	1.74	94.89
3	1.24	96.36
5	0.38	98.88
10	0.28	99.18
20	0.47	98.62
40	0.42	98.77
60	0.53	98.44
90	0.33	99.03
123	0.78	97.71

Table S8. Kinetic fitting parameters of $[(CH_3)_2NH_2][Zr(PO_4)F_2]$ for Sr^{2+} removal (m/V = 1 g L^{-1}, at room temperature).

kinetic model	k_1 (min^{-1})	k_2 (g mg^{-1} min^{-1})	q_e^{Sr} (mg L^{-1})	R^2
Pseudo-first-order model	3.3364	-	33.49	0.6429
Pseudo-second-order model	-	0.7119	33.62	0.7695

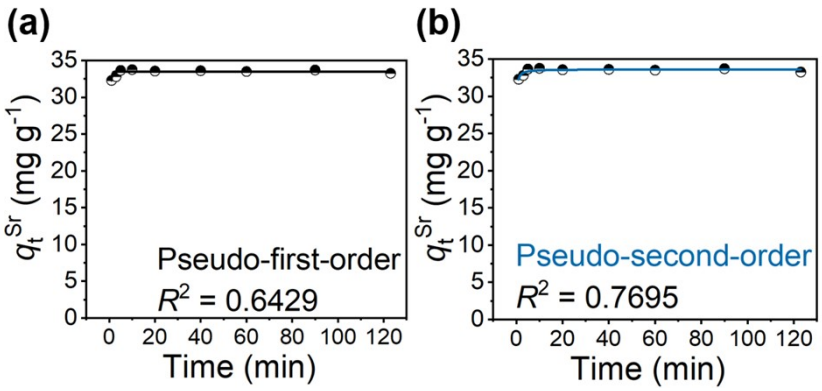

Figure S2. The $[(CH_3)_2NH_2][Zr(PO_4)F_2]$ kinetics data fitted by the pseudo-first-order model (**a**) and the pseudo-second-order model (**b**) using nonlinear equation.

Table S9. The Sr^{2+} adsorption results and Zr leaching percentage of $[(CH_3)_2NH_2][Zr(PO_4)F_2]$ (m/V = 1 g L^{-1}, at room temperature and 12 h contact time) across pH = 0.92 – 12.92.

pH	C_0^{Sr} (mg L^{-1})	C_e^{Sr} (mg L^{-1})	K_d^{Sr} (mL g^{-1})	R^{Sr} (%)	Average dissolution concentration of Zr (mg L^{-1})	Average leaching percentage of Zr (%)
0.92	11.19	7.77	4.40×10^2	30.56	52.96	15.69
1.95	11.12	1.78	5.25×10^3	83.99	22.28	6.60
2.98	11.54	1.80	5.41×10^3	84.40	6.14	1.82
4.02	11.75	1.17	9.04×10^3	90.04	6.72	1.99
4.83	11.61	0.71	1.54×10^4	93.88	7.53	2.23
5.37	11.29	0.47	2.30×10^4	95.84	6.92	2.05
6.53	11.62	0.45	2.48×10^4	96.13	2.18	0.65
7.36	14.15	0.99	1.33×10^4	93.00	4.00	1.19
8.46	11.64	0.99	1.08×10^4	91.49	6.86	2.03
9.54	11.28	2.31	3.88×10^3	79.52	7.53	2.23
10.91	11.68	2.33	4.01×10^3	80.05	7.84	2.32
11.87	11.58	3.25	2.56×10^3	71.93	19.08	5.65
12.92	11.79	3.53	2.34×10^3	70.06	47.49	14.07

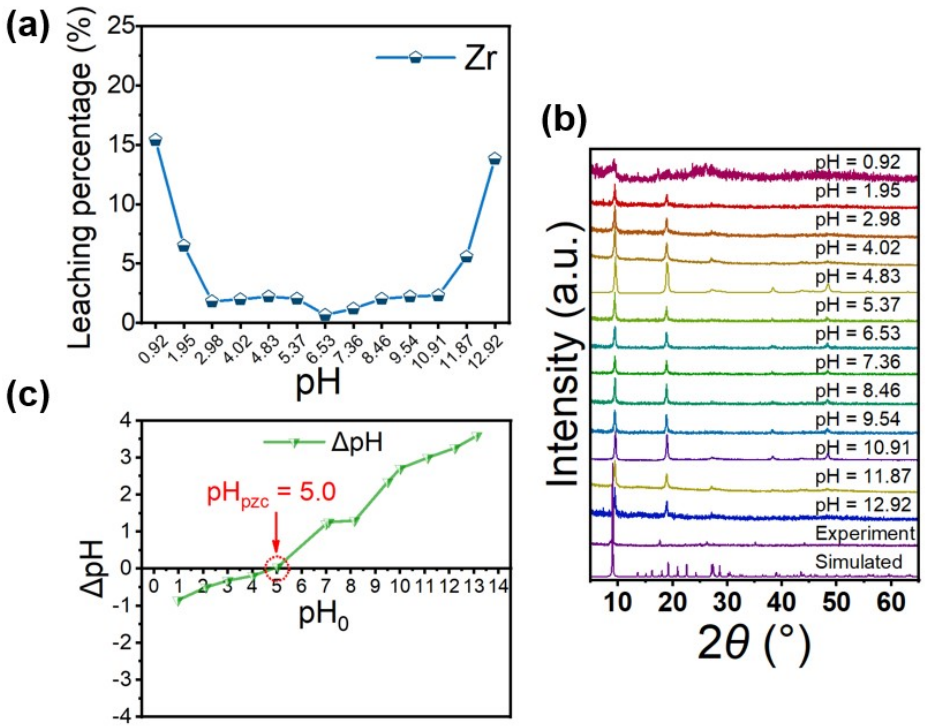

Figure S3. (**a**) Zr leaching percentage curves of $[(CH_3)_2NH_2][Zr(PO_4)F_2]$ treated with different pH solutions. (**b**) PXRD patterns of $[(CH_3)_2NH_2][Zr(PO_4)F_2]$ synthesized and its corresponding samples in Sr^{2+} solutions with different pH values. (**c**) The determination of pH_{pzc} for $[(CH_3)_2NH_2][Zr(PO_4)F_2]$ in aqueous solutions.

Table S10. The adsorption results of $[(CH_3)_2NH_2][Zr(PO_4)F_2]$ under different Na^+/Sr^{2+} molar ratios (m/V = 1 g L^{-1}, at room temperature and 12 h contact time).

Molar ratio (Na^+/Sr^{2+})	C_0^{Na} (mg L^{-1})	C_e^{Na} (mg L^{-1})	C_0^{Sr} (mg L^{-1})	C_e^{Sr} (mg L^{-1})	K_d^{Sr} (mL g^{-1})	K_d^{Na} (mL g^{-1})	R^{Sr} (%)	$SF_{Sr/Na}$
4.8	6.92	5.72	5.55	0.020	2.77×10^5	209.79	99.64	1317.98
178.3	224.55	197.78	4.80	0.022	2.17×10^5	135.35	99.54	1604.57
494.4	455.31	424.96	3.51	0.022	1.59×10^5	71.42	99.37	2219.95
1190.6	1737.00	1674.50	5.56	1.52	2.66×10^3	37.32	72.66	71.21

Table S11. The adsorption results of $[(CH_3)_2NH_2][Zr(PO_4)F_2]$ under different K^+/Sr^{2+} molar ratios (m/V = 1 g L^{-1}, at room temperature and 12 h contact time).

Molar ratio (K^+/Sr^{2+})	C_0^{K} (mg L^{-1})	C_e^{K} (mg L^{-1})	C_0^{Sr} (mg L^{-1})	C_e^{Sr} (mg L^{-1})	K_d^{Sr} (mL g^{-1})	K_d^{K} (mL g^{-1})	R^{Sr} (%)	$SF_{Sr/K}$
45.6	107.34	71.53	5.28	0.13	3.96×10^4	500.63	97.54	79.13
118.7	294.91	235.16	5.57	0.20	2.69×10^4	254.08	96.41	105.67
568.9	1104.34	1042.29	4.35	1.26	2.45×10^3	59.53	71.03	41.19
1422.3	2690.96	2631.16	4.24	1.66	1.55×10^3	22.73	60.85	68.39

Table S12. The adsorption results of $[(CH_3)_2NH_2][Zr(PO_4)F_2]$ under different Mg^{2+}/Sr^{2+} molar ratios (m/V = 1 g L^{-1}, at room temperature and 12 h contact time).

Molar ratio (Mg^{2+}/Sr^{2+})	C_0^{Mg} (mg L^{-1})	C_e^{Mg} (mg L^{-1})	C_0^{Sr} (mg L^{-1})	C_e^{Sr} (mg L^{-1})	K_d^{Sr} (mL g^{-1})	K_d^{Mg} (mL g^{-1})	R^{Sr} (%)	$SF_{Sr/Mg}$
20.1	27.64	19.88	4.96	0.042	1.17×10^5	390.34	99.15	299.98
81.0	101.75	61.23	4.53	0.024	1.88×10^5	661.77	99.47	283.71
211.4	292.51	260.22	4.99	2.53	9.72×10^2	124.09	49.30	7.84
538.4	724.12	693.84	4.85	3.89	2.47×10^2	43.64	19.79	5.65

Table S13. The Sr^{2+} adsorption results of $[(CH_3)_2NH_2][Zr(PO_4)F_2]$ under different $Na^+/K^+/Cs^+/Sr^{2+}$ molar ratios (m/V = 1 g L^{-1}, at room temperature and 12 h contact time).

Molar ratio (M/Sr^{2+})	Ions	C_0^M (mg L^{-1})	C_e^M (mg L^{-1})	K_d^M(mL g^{-1})	R^M (%)	$SF_{Sr/M}$
1	Sr^{2+}	5.12	0.089	5.65×10^4	98.26	-
51.1	Na^+	68.64	63.30	8.44×10^1	7.78	670.08
12.5	K^+	28.49	18.28	5.59×10^2	35.84	101.21
4.3	Cs^+	33.54	9.44	2.55×10^3	71.85	22.14
Molar ratio (M/Sr^{2+})	**Ions**	**C_0^M (mg L^{-1})**	**C_e^M (mg L^{-1})**	**K_d^M(mL g^{-1})**	**R^M (%)**	**$SF_{Sr/M}$**
1	Sr^{2+}	5.34	0.19	2.71×10^4	96.44	-
125.3	Na^+	168.39	161.83	4.05×10^1	3.90	668.67
55.3	K^+	126.30	109.20	1.57×10^2	13.54	173.09
17.7	Cs^+	137.18	86.08	5.94×10^2	37.25	45.66

Table S14. The removal efficiencies of $[(CH_3)_2NH_2][Zr(PO_4)F_2]$ under $Cs^+/K^+/Na^+/Ca^{2+}/Mg^{2+}/Sr^{2+}$ molar ratio of 0.6/17.8/54.0/8.6/5.0/1 (m/V = 1 g L^{-1}, at room temperature and 12 h contact time).

Molar ratio (M/Sr^{2+})	Ions	C_0^M (mg L^{-1})	C_e^M (mg L^{-1})	K_d^M(mL g^{-1})	R^M (%)	$SF_{Sr/M}$
1	Sr^{2+}	3.35	0.45	6.44×10^3	86.57	-
0.6	Cs^+	3.10	0.91	2.41×10^3	70.65	2.68
17.8	K^+	26.63	12.99	1.05×10^3	51.22	6.14
54.1	Na^+	47.55	46.90	1.40×10^1	1.37	464.99
8.6	Ca^{2+}	13.19	6.95	8.98×10^2	47.31	7.18
5.0	Mg^{2+}	4.61	1.30	2.55×10^3	71.80	2.53

Table S15. The results on Sr^{2+} ions removal by $[(CH_3)_2NH_2][Zr(PO_4)F_2]$ in actual water samples contaminated with Sr^{2+} ions (m/V = 1 g L^{-1}, at room temperature and 12 h contact time).

Water	C_0^{Sr} (mg L^{-1})	C_e^M (mg L^{-1})	K_d^M (mL g^{-1})	R^{Sr} (%)
Tap water (Fuzhou, Fujian)	5.47	0.05	1.08×10^5	99.09
River water (Fuzhou, Fujian)	5.43	0.09	5.93×10^4	98.34
Lake water (Qishan Lake, Fuzhou, Fujian)	5.71	0.06	9.42×10^4	98.95
Seawater (Dongshan Island, Zhangzhou, Fujian)	6.59	1.38	3.78×10^3	79.06

Table S16. The adsorption and desorption results for $[(CH_3)_2NH_2][Zr(PO_4)F_2]$ at one cycle (m/V = 1 g L^{-1}, at room temperature and 12 h contact time).

Adsorption					Desorption			
m (mg)	V (mL)	C_0^{Sr} (mg L^{-1})	C_e^{Sr} (mg L^{-1})	R^{Sr} (%)	m_1 (mg)	V_1 (mL)	C_e^{Sr} (mg L^{-1})	E^{Sr} (%)
50	50	11.62	0.72	93.80	20	20	9.97	91.47

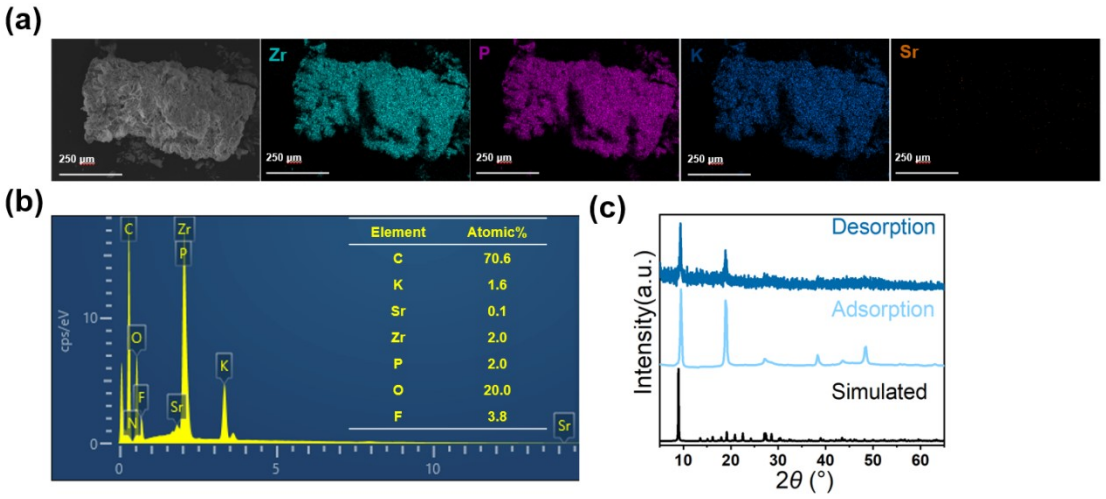

Figure S4. (**a**) Elemental distribution mappings and (**b**) EDS analysis results of the material after desorption. (**c**) PXRD patterns of $[(CH_3)_2NH_2][Zr(PO_4)F_2]$ after Sr^{2+} adsorption and desorption.

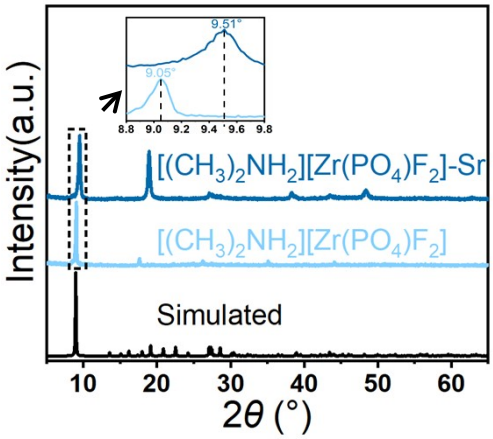

Figure S5. Simulated and experimental PXRD patterns for pristine $[(CH_3)_2NH_2][Zr(PO_4)F_2]$ and experimental PXRD pattern of $[(CH_3)_2NH_2][Zr(PO_4)F_2]$-Sr.

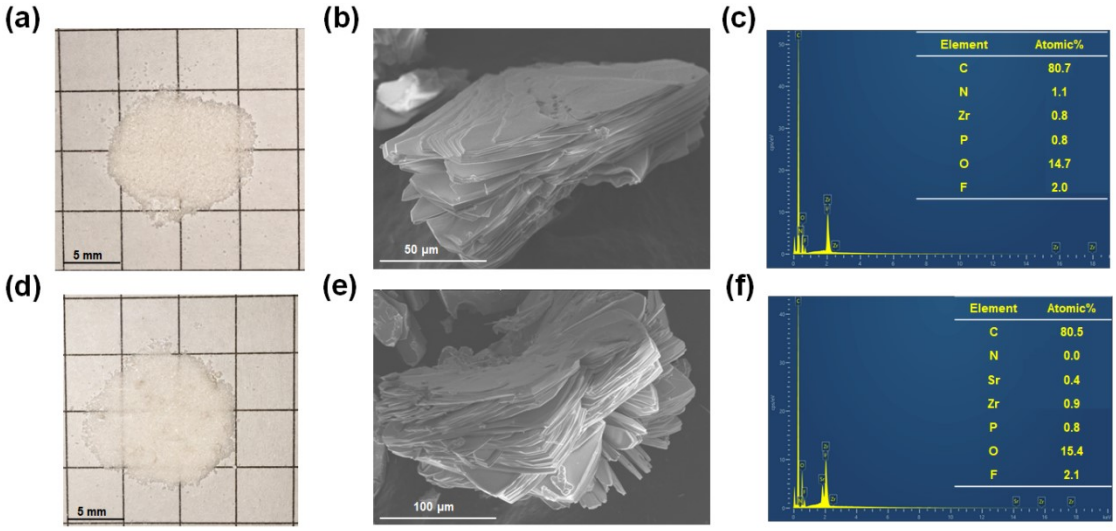

Figure S6. The photograph (**a**), SEM images at magnification of 800 (**b**), and EDS analysis results (**c**) of $[(CH_3)_2NH_2][Zr(PO_4)F_2]$. The photograph (**d**), SEM images at magnification of 450 (**e**), and EDS analysis results (**f**) of $[(CH_3)_2NH_2][Zr(PO_4)F_2]$-Sr.

Table S17. Thermodynamics data of Sr^{2+} adsorption by $[(CH_3)_2NH_2][Zr(PO_4)F_2]$ under different temperature conditions (m/V = 1 g L^{-1}, 12 h contact time).

T (K)	C_0^{Sr} (mg L^{-1})	C_e^{Sr} ()	K_d (mL g^{-1})	ΔH^0 (kJ mol^{-1})	ΔS^0 (kJ mol^{-1} K^{-1})	ΔG^0 (kJ mol^{-1})
293	9.82	1.01	8.72×10^3	29.62	0.18	-22.10
313	10.39	0.56	1.76×10^4			-25.43
333	10.21	0.24	4.15×10^4			-29.44
353	9.98	0.15	6.55×10^4			-32.55

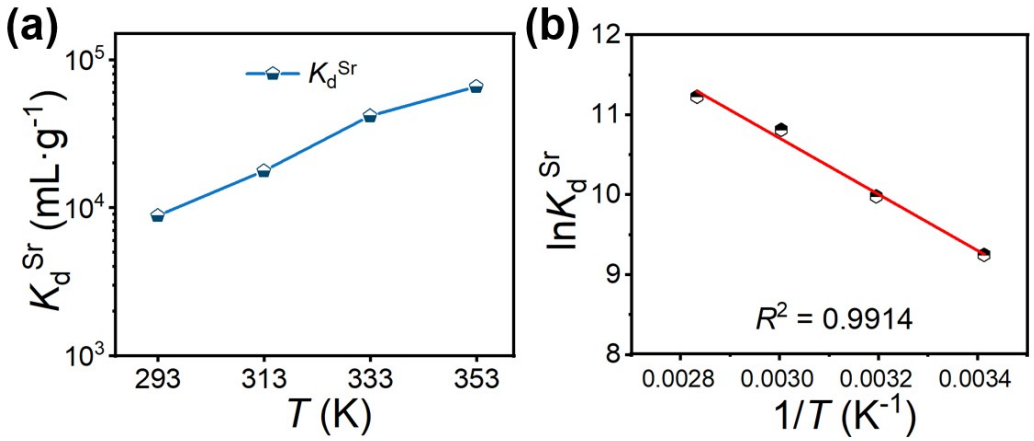

Figure S7. K_d *vs.* T (**a**) and lnK_d *vs.* 1/T (**b**) for Sr^{2+} adsorption by $[(CH_3)_2NH_2][Zr(PO_4)F_2]$ at various temperatures.

Notes and references

1. K. Sakadevan and H. J. Bavor, *Water Res.*, 1998, **32**, 393-399.
2. Y. S. Ho, D. A. J. Wase and C. F. Forster, *Environ. Technol.*, 1996, **17**, 71-77.
3. M. A. Salam and R. C. Burk, *Appl. Surf. Sci.*, 2008, **255**, 1975-1981.
4. A. Dabrowski, P. Podkoscielny, Z. Hubicki and M. Barczak, *Chemosphere*, 2005, **58**, 1049-1070.
5. J. R. Zhang, L. Chen, X. Dai, L. X. Chen, F. W. Zhai, W. F. Yu, S. K. Guo, L. J. Yang, L. H. Chen, Y. G. Zhang, L. W. He, C. L. Chen, Z. F. Chai and S. Wang, *Chem. Commun.*, 2021, **57**, 8452-8455.
6. J. Zhang, L. Chen, X. Dai, L. Zhu, C. Xiao, L. Xu, Z. Zhang, E. V. Alekseev, Y. Wang, C. Zhang, H. Zhang, Y. Wang, J. Diwu, Z. Chai and S. Wang, *Chem*, 2019, **5**, 977-994.
7. J. R. Zhang, L. H. Chen, D. X. Gui, H. W. Zhang, D. Zhang, W. Liu, G. L. Huang, D. W. Juan, Z. F. Chai and S. Wang, *Dalton Trans.*, 2018, **47**, 5161-5165.
8. Y. Cheng, I. bin Samsudin, S. Jaenicke and G. K. Chuah, *Chem. - Asian J.*, 2020, **15**, 3542-3550.
9. D. Sarma, C. D. Malliakas, K. S. Subrahmanyam, S. M. Islama and M. G. Kanatzidis, *Chem. Sci.*, 2016, **7**, 1121-1132.
10. J. L. Mertz, Z. H. Fard, C. D. Malliakas, M. J. Manos and M. G. Kanatzidis, *Chem. Mater.*, 2013, **25**, 2116-2127.
11. M. J. Manos, N. Ding and M. G. Kanatzidis, *Proc. Natl. Acad. Sci. U.S.A.*, 2008, **105**, 3696-3699.
12. X. H. Qi, K. Z. Du, M. L. Feng, J. R. Li, C. F. Du, B. Zhang and X. Y. Huang, *J. Mater. Chem. A*, 2015, **3**, 5665-5673.
13. J. Zhang, L. Chen, L. Chen, L. Chen, Y. Zhang, C. Chen, Z. Chai and S. Wang, *Dalton Trans.*, 2022, **51**, 14842-14846.
14. S. Bevara, P. Giri, S. J. Patwe, S. N. Achary, R. K. Mishra, A. Kumar, A. K. Sinha, C. P. Kaushik and A. K. Tyagi, *J. Environ. Chem. Eng.*, 2018, **6**, 2248-2261.
15. L. A. Wu, H. P. Wang, X. Q. Kong, H. B. Wei, S. Chen and L. S. Chi, *RSC Adv.*, 2023, **13**, 6346-6355.
16. J. Gu, S. Du, Q. Yu and W. Mu, *Chem. Res. Appl.*, 2020, **32**, 1067-1071.
17. S. Inan and E. Nostar, *Sep. Sci. Technol.*, 2013, **48**, 1364-1369.
18. Y. Park, Y. C. Lee, W. S. Shin and S. J. Choi, *Chem. Eng. J.*, 2010, **162**, 685-695.